Vibrational Study of SO_x Adsorption on Pt/SiO_2

Djamela Bounechada,[†,¶] Zhafira Darmastuti,[‡] Mike Andersson,[‡] Lars Ojamäe,[‡]

Anita Lloyd Spetz,[‡] Magnus Skoglundh,[†] and Per-Anders Carlsson[*,†]

Department of Chemical and Biological Engineering and Competence Centre for Catalysis, Chalmers University of Technology, SE-412 96 Göteborg, Sweden, and Department of Physics, Chemistry and Biology, Linköping University, SE-581 83 Linköping, Sweden

E-mail: per-anders.carlsson@chalmers.se

Phone: +46 (0)708 720287. Fax: +46 (0)31 160062

Abstract

The formation of ad-SO_x species on Pt/SiO_2 upon exposure to SO_2 in concentrations ranging from 10 to 50 ppm at between 200 and 400°C has been studied by *in situ* diffuse reflectance infrared Fourier transformed spectroscopy. In parallel, first-principles calculations have been carried out to consolidate the experimental interpretations. It was found that sulfate species form on the silica surface with a concomitant removal/rearrangement of silanol groups. Formation of ad-SO_x species occurs only after SO_2 oxidation to SO_3 on the platinum surface. Thus SO_2 oxidation to SO_3 is the first step in the SO_x adsorption process, followed by spillover of SO_3 to the oxide and, finally, the formation of sulfate species on the hydroxyl positions on the oxide. The sulfate formation is influenced by both temperature and SO_2 concentration.

[*]To whom correspondence should be addressed

[†]Department of Chemical and Biological Engineering and Competence Centre for Catalysis, Chalmers University of Technology, SE-412 96 Göteborg, Sweden

[‡]Department of Physics, Chemistry and Biology, Linköping University, SE-581 83 Linköping, Sweden

[¶]Current address: Johnson Matthey Technology Centre, Blount's Court, Sonning Common, Reading RG4 9NH, United Kingdom

Furthermore, exposure to hydrogen is shown to be sufficiently efficient as to remove ad-SO_x species from the silica surface.

Keywords: Chemical sensors; SiC-FET; Surface reactions; Supported platinum; Sulfur

Introduction

Emissions of sulfur dioxide (SO_2) are harmful both to the human health and the environment. A significant part of the SO_2 emissions originates from thermal power generation during the combustion of sulfur-containing fuels. Before venting the flue gas from such combustion processes to the atmosphere, SO_2 is usually removed by desulfurization in a scrubber. Herein the flue gas is treated with lime slurry to form gypsum that is collected at the bottom of the scrubber while the cleaned flue gas is vented to the atmosphere at the top. In addition to lime slurry, there are numerous of other absorbents for SO_2 removal such as dry lime or seawater with high alkalinity. For efficient desulfurization, both the concentration and distribution of SO_2 in the desulfurization unit are important parameters to measure. In this connection, sensors as part of the process control system play a decisive role in the optimization of the desulfurization process.

To enable installation of multiple sensors in the flue gas duct, small and cheap sensor devices need to be developed. Several studies have been performed to investigate potential sensors for this application. The silicon carbide field-effect transistor (SiC-FET) sensors are among the most promising candidates because such devices can be operated at high temperature, low oxygen concentration and harsh industrial environments.[1,2] SiC-FET sensors have already shown promising results in industrial applications for detection and control of ammonia[3] and carbon monoxide.[4,5] More recently, efforts to develop SiC-FET sensors for SO_2 detection in desulfurization systems have been performed.[6] The response of this type of device depends on the adsorption and subsequent chemical reactions of the flue gas compounds on the surface of the sensor. The sensitivity and selectivity of SiC-FET sensors can be tuned by changing the material of the catalytic metal gate,[4] the gate insulator,[7] the morphology of the gate,[8,9] the operating temperature[4] and the bias

voltage on the substrate[10] or the gate.[8,11] For the gas sensor considered in the present study, the gate material is a porous thin layer of platinum on top of silicon dioxide as gate oxide. The surface of this type of sensor is illustrated in **??**a and b.

Understanding the detection mechanism of the sensor is crucial for the development of efficient sensors. Of particular importance is to map out the adsorption properties and chemical reactions proceeding on the surface of the sensor gate in order to improve the sensing performance. Previous studies, with integrated *in situ* diffuse reflectance infrared Fourier transformed spectroscopic (DRIFTS) measurements and theoretical modeling, show that the detection of hydrogen involves adsorption and subsequent dissociation of the hydrogen molecule on the catalytic metal gate, followed by diffusion of the hydrogen atoms/ions to the insulator. The latter create a polarized layer of hydroxyl groups and the resulting electric field changes the conductivity of the channel underneath the gate.[1,12] The formation of hydroxyl groups was revealed by vibrational frequency studies of the interaction of hydrogen-containing species on the Pt/SiO_2 system.[13,14] In these studies high-surface area silica impregnated with platinum was used as a model for the sensor surface(s) in order to facilitate a reasonable signal-to-noise ratio in the direct measurements of adsorbed species with DRIFTS.

The detection mechanism of non-hydrogen compounds as carbon monoxide (CO) and sulfur oxides (SO_x) is not as straightforward. A previous study of the detection mechanism of CO on a Pt/SiO_2 SiC-FET sensor[15] showed that the sensor response is influenced by several factors. A strong correlation was observed between the sensor response and the coverage of CO on the surface of the sensor. In fact, the CO/O coverage influences the oxidation state of Pt at the surface and therefore also the electrical characteristics of the device. Furthermore, catalytic CO oxidation on Pt may promote spillover/reverse spillover of oxygen between the Pt and the oxide, which may play a role in the detection mechanism.

The aim of the present work is to study the interaction of SO_2 with Pt/SiO_2 and the subsequent formation of ad-SO_x species upon exposure to SO_2 concentrations for which SiC-FET sensors show good response.[6] Thus we have carried out experiments with SO_2 concentrations between 10

and 50 ppm both in absence and presence of oxygen in the temperature range of 200-400°C and used DRIFTS to characterize the surface species *in situ*. In parallel first-principles calculations have been performed to scrutinize the vibrational frequencies of several species that might be present on the surface to guide the assignment of surface species and strengthen the experimental findings.

Experimental and theoretical methods

Sample preparation and characterization

The details on the preparation and characterisation of the Pt/SiO_2 sample can be found elsewhere [16] and thus we give only a brief description here. Silica powder (Kromasil Silica KR-300-10, Akzo Nobel Eka Chemicals) was pretreated in air at 600°C for 2 hours. The 4 wt.-% Pt/SiO_2 sample was then prepared according to the incipient wetness impregnation technique, by dispersion of the support material in an aqueous solution of tetraammineplatinum(II)nitrate ($(NH_3)_4Pt(NO_3)_2$, Alfa Aesar GmbH & Co. KG). In order to increase the interaction between the platinum precursor and the support material, the pH of the solution was adjusted to 11 by NH_4OH addition. [17] After stirring (20 minutes), the sol was instantly frozen with liquid nitrogen, freeze-dried for 12 hours and finally calcined in air at 500°C for one hour using a heating rate of 5°C/min.

The surface area of the sample was measured with nitrogen physisorption and the specific surface area was calculated to be 117 m^2/g according to the BET method for P/P_0 = 0.05-0.20. The sample was also studied by scanning transmission electron microscopy (STEM), using an FEI Titan 80-300 TEM with a probe Cs (spherical aberration) corrector operated at 300 kV and a high-angle annular dark field (HAADF) STEM imaging mode providing Z number contrast. The sample contains platinum particles with diameters ranging from one to ten nm, with about 40% below three nm. The corresponding dispersion of platinum is about 7%.

Experimental equipment and procedures

The *in situ* infrared Fourier transformed spectroscopic measurements were performed in diffuse reflectance mode using a Bio-Rad FTS6000 spectrometer equipped with a high-temperature stainless steel reaction cell (Harrick Scientific, Praying Mantis) coated with Silcolloy 1000 (SilcoTek) and provided with KBr windows and a nitrogen cooled MCT detector. The temperature of the sample holder was measured by a thermocouple (k-type) and controlled by a PID regulator (Eurotherm 3216). Individual mass flow controllers (Bronkhorst LOW-ΔP-FLOW) were used to introduce the gases. Moreover the O_2 feed was introduced via an air actuated high-speed gas valve (Valco, VICI), in order to provide precise transients. The outlet gas composition was analyzed by mass spectrometry (Balzers QuadStar 420) following the m/z 2 (H_2), 18 (H_2O), 28 (CO), 32 (O_2 and S), 33 (HS), 34 (H_2S), 40 (Ar), 44 (CO_2), 48 (SO), 64 (SO_2) 80 (SO_3), 81 (SO_3), 82 (SO_3) and 83 (SO_3).

The 4% Pt/SiO_2 sample was first mixed with natural diamond powder (40-60 μm, Alfa Aesar GmbH & Co KG), using a sample:diamond wt.-ratio of 1:4. The diluted sample was then pressed into tablets, ground in an agate mortar and sieved before analysis. Only particles larger than 38 μm were used for the DRIFTS experiments. For the experiments performed using silica-only, the pretreated silica powder was pressed into tablets, ground in an agate mortar and sieved. Then the fraction of particles with size between 40 and 100 μm was mixed with natural diamond powder using a silica:diamond ratio of 1:4.

A schematic description of the SO_x adsorption experiments is given in **??**. Before each experiment the sample was treated at 400°C with 10 vol.-% O_2 in Ar for 10 min (oxidation) and then with 4 vol.-% H_2 in Ar for 10 min (reduction), using a total flow of 100 ml/min. After the pre-treatment the sample was cooled in Ar (cooling rate of 10°C/min) until reaching the temperature at which the experiment was performed, *i.e.* 200, 300 or 400°C. The isothermal experiment was started, after 20 min dwelling in Ar, by feeding SO_2 for 15 min and then introducing O_2 (10 vol.%) together with SO_2 in the feed gas mixture for 15 min. Three different SO_2 levels (10, 30 or 50 ppm) were investigated in independent experiments at each temperature. Finally, after each experiment the sample

was regenerated at 400°C with 4 vol.-% H_2 in Ar for 10 min. In order to investigate possible effects of the diluent and reaction cell, three blank experiments were performed exposing natural diamond, pre-mixed with 1 wt.% high-surface area platinum black (Alfa Aesar GmbH & Co KG), to 50 ppm SO_2 in absence and presence of 10% oxygen at 200, 300 and 400°C. The role played by the noble metal was also investigated by performing the same experiment using a sample of the bare support material (silica) diluted in diamond. The reference spectrum used for the background subtraction was collected 10 min before the introduction of SO_2 in the feed gas mixture. Sample spectra were then collected every 30 seconds starting 2 min before the introduction of SO_2. The wavenumber region 1000-4000 cm^{-1} was investigated with a spectral resolution of 1 cm^{-1}.

First-principles calculations

Quantum chemical calculations were performed to study vibrational frequencies of potential species adsorbed on the sensor surface. The Gaussian03 program[18] with the B3LYP[19] hybrid density functional was employed for the calculations. A mixture of two basis sets was used for these calculations: the 6-311++G (2d, 2p)[20] and the LanL2DZ[21] basis sets. The larger basis set, 6-311++G (2d, 2p) is more accurate, but it is not available for Pt. Therefore, a mixed basis consisting of LanL2DZ for Pt and 6-311++G (2d, 2p) for other species was utilized for this study. The smaller basis set used for Pt may slightly affect the adsorption energies involving the Pt clusters, but not much for the vibrational frequency, which is the focus in the calculations. A convergence test was performed as to compare the results of the calculations with previously reported values. This is described in Table S1 to S3 in the supporting information.

As shown in **??**a the structures of the silica clusters are represented by a $Si(OH)_4$ cluster from Wallin *et al.*[22] and by a cluster cut out from the structure of β-Cristobalite,[23] respectively. The β-Cristobalite structure was chosen because the cluster provides a more realistic structure for the SiO_2 surface, and exhibits a higher stability due to its larger size. Additionally, it presents on its surface different types of hydroxyl groups that can act as adsorption sites for SO_2. Two types

of Pt clusters were used in the simulations. The first is a Pt_4 cluster, with corners consisting of single atomic Pt, to model the interaction between the gas and a Pt atom. The second is a larger Pt_{22} cluster to represent a Pt (111) surface. The geometries of these structures were optimized to calculate the structures and ground state energies of different species during the gas-metal-oxide interaction. In addition, a model was also employed to simulate diamond-SO_2 interactions. The dangling bonds in diamond were terminated with OH- and H-groups.[24]

In this study computations were performed to calculate both the adsorption energy between SO_2 and the Pt/SiO_2 surface, and the IR vibrational frequencies. Local energy-minimum structures were derived by performing geometry optimizations using the Gaussian03 program where the atomic positions in the initial structures (positions as in the crystal structures) were allowed to relax to diminish the energy. The adsorption energies were computed from the electronic energy of the geometry-optimized products minus the sum of the electronic energies of the geometry-optimized reactants, the product being the complex of a Pt or silica cluster and the adsorbed molecule and the two reactants being the pure cluster and the free molecule. The IR spectra were obtained from normal-mode calculations for the geometry-optimized structures using the same basis sets as above.

Results

SO_x adsorption on 4% Pt/SiO_2

The SO_x adsorption experiments with the 4%Pt/SiO_2 sample were all carried out using natural diamond as diluent. Despite this, nearly complete absorption of infrared radiation is observed in the region 1000-1200 cm^{-1} and thus this region is omitted in the following analysis (*cf.* Figure S1). Further, it is worth mentioning that the response signals for all reference spectra, *i.e.*, before SO_x exposure, are similar (*cf.* Figure S1). This supports that the sample regeneration procedure carried out between the SO_x adsorption experiments works well. The *in situ* DRIFTS results of the SO_x adsorption experiments at 200, 300 and 400°C are shown in **??** and **??**. **??** shows the IR

spectra collected after 15 min of exposure to SO_2 and after further 15 min of exposure to SO_2 in the presence of 10% O_2, between 4000-2600 and 1650-1200 cm^{-1}. The IR spectra reported hereafter are solely the current spectra subtracted from the corresponding background spectra (*cf.* Figure S1). The evolution of the absorption bands related to sulfates (1480-1350 cm^{-1}) and terminal silanols (3900-3400 cm^{-1}) are displayed in **??**. In order to facilitate the interpretation of the results, assignments of IR bands for sulfur-containing species, water and silanols are summarized in **??**, together with the corresponding literature references. A common feature of all SO_x adsorption experiments performed is the lack of absorption bands in the difference IR spectrum collected after 15 min of SO_2 exposure (dotted lines in **??**). This suggests that the exposure to SO_2 alone does not modify the surface species present on the pre-treated sample.

After further 15 min of exposure to 10 ppm SO_2 in the presence of 10% O_2 at 200°C (**??**a) two positive absorption bands appear at 1424 and 1336 cm^{-1}, accompanied by two negative absorption bands at 3717 and 3531 cm^{-1}. The first band is close to that observed by Anderson *et al.*[25] for sulfate species (SO_4^{2-}) on silica, while the two negative bands previously have been assigned to *isolated*[26] and *vicinal* (H-bonded)[13] silanols (SiOH), respectively (*cf.* **??**). More difficult to interpret is the absorption band at 1336 cm^{-1}, which could be due to SO_2 adsorbed on the surface of either silica[27] or diamond.[28] A positive broad band is also observed between 3420 and 2600 cm^{-1}, with a maximum at 2660 cm^{-1}. This might be related to a combination of OH stretching mode of perturbed hydroxyl groups on silica[26] (*cf.* **??**) and SH stretching mode of SiSH.[29] However, the band is not very pronounced. Moreover, a small positive peak, which we assign to the deformation vibration of condensed water, is detected at around 1594 cm^{-1} together with two series of negative sharp rotational bands between 3905-3540 cm^{-1} and 1900-1450 cm^{-1}, which are characteristic for gaseous water.[13] The same absorption bands are observed during the corresponding experiments with 30 and 50 ppm SO_2, with slightly increasing intensity with increasing SO_2 concentration. As regarding the integrated peak area for sulfates on silica (1480-1350 cm^{-1}), it remains constant (and close to zero) during SO_2 exposure and starts to increase as soon as O_2 is introduced in the feed (**??**a). Furthermore, the higher integrated area is obtained during exposure of the sample to

the higher SO_2 concentration. In a specular way, the integrated peak area for terminal silanols (3900-3400 cm^{-1}) remains constant (and close to zero) for the first 15 min of SO_2 exposure and continuously decreases when introducing O_2 in the feed (**??**a). In this case the integrated area is more negative in correspondence with the higher SO_2 concentration. The changes in the IR absorption bands upon introduction of oxygen are accompanied by a minimum in outlet SO_2 concentration, which is most clear in the experiment with 30 and 50 ppm SO_2 in the feed. This is clear from **??** showing the outlet SO_2 concentration measured during the SO_2 adsorption experiments with different concentrations of SO_2. The first ten minutes of the experiment shows the period with only Ar in the feed. At t=10 min SO_2 is introduced to the feed, which results in an increase in the outlet SO_2 concentration towards the inlet feed concentration, *i.e.*, 10, 30 or 50 ppm. As can be seen the outlet SO_2 concentration reaches no stable levels during the 15 min period. This is an artifact caused mainly by the gas system downstream the reactor cell and also the gas inlet system on the mass spectrometer. Control experiments, *i.e.*, SO_2 step-response experiments while bypassing the reaction cell, showed that it takes about 15 min to detect a stable SO_2 level. This means that the SO_2 response should not be used as a basis for, *e.g.*, SO_2 storage during the oxygen-free periods. However, continuing the experiment by adding also oxygen at t=25 min results in a minimum in the detected outlet SO_2 concentration. This is, at least qualitatively, a real effect and not an artifact caused by the gas system design. The minimum reflects both oxidation of SO_2 into SO_3 (which could not be resolved properly with the present mass spectrometer as SO_3 may fragment to SO_2) and storage of SO_3 as observed by IR. We mention that a quantitative analysis of SO_x storage is not straightforward from the present data due to uncertainties about the gas system SO_2. However, the minimum supports that oxygen is needed to adsorb SO_2 and supports the IR results well.

Since the results of the experiments performed at 300 and 400°C are qualitatively similar (**??** b and c), they will be described together. Similarly to the experiments at 200°C, after 15 min of exposure to 10 ppm SO_2 an absorption band at 1415 cm^{-1} appears, accompanied by two negative absorption bands at 3730 and 3536 cm^{-1}. In these experiments a tiny positive peak at 3745 cm^{-1} can also be observed. Once again we can easily assign the first band to surface sulfates on silica[25]

and the two negative bands to *isolated*[30] and *vicinal* (H-bonded)[13] silanols, respectively, whereas the peak at 3745 cm^{-1} might be due to the formation of *geminal* hydroxyl species on silica.[31] A series of overlapped positive bands appear between 1360 and 1200 cm^{-1}, likely due to a combination of different sulfur containing species. In particular, the absorption band at 1328 cm^{-1} (already observed during the experiments performed at 200°C) could be due to SO_2 adsorbed on the surface of either silica[27] or diamond.[28] The positive broad absorption band centered at 1286 cm^{-1}, which is observed only at 400°C, is more difficult to assign. It might be due to the stretching mode of C=S in *trans*-HSCS,[32] but it is also characteristic of both deformation mode of HCS in *trans*-HCSSH[32] and stretching mode of SiS in silicon oxysulfide species (OSiS).[33] Finally, the positive bands at 1237 and 1232 cm^{-1}, in the experiments performed at 300 and 400°C, respectively, might be related either to *trans*-HSCS species[32] or to the SiOSi asymmetric stretching of silica.[29] Alternatively, adsorbed SO_2 species on platinum have been reported to show characteristic absorption bands in the wavenumber range 1300-1100 cm^{-1}.[34] Two new positive broad absorption bands appear at 3261 and 3090 cm^{-1} when exposing the sample to higher SO_2 concentrations at 400°C, which are difficult to assign. A broad band around 3250 cm^{-1} was previously observed for high-silica-containing zeolites by Zholobenko *et al.*[35] and assigned to a complex with a hydrogen bond between acidic OH groups and one lattice oxygen atom. Furthermore, bands at 3100 and 3050 cm^{-1}, ascribed to OH groups which form a hydrogen bond with the oxygen atom of water, were observed by Karyakin *et al.*[36] The peaks at 3261 and 3090 cm^{-1} might also be due to perturbed silanols[26] H-bonded to an oxygen atom of sulfates (*cf.* **??**) or to C-H stretching mode[37] [40] of diamond species. Once again the integrated peak areas for the experiments at 300 and 400°C remain constant (and close to zero) during SO_2 exposure. Then, as soon as O_2 is introduced, increasing and decreasing trends are observed for sulfates on silica (1480-1350 cm^{-1}) and for the terminal silanol groups (3900-3400 cm^{-1}), respectively, always converging to an asymptotic value (*cf.* **??**b and c). Once again the most pronounced changes in the integrated areas are obtained when exposing the sample to the higher SO_2 concentration and the changes are accompanied by a minimum in outlet SO_2 concentration (*cf.* **??**).

By comparing the IR spectra collected at the end of each experiment performed at different temperatures but at parity of inlet SO_2 concentration, it can be noticed that the higher intensity for the IR band related to sulfates on silica (around 1430 cm^{-1}) is always obtained at 300°C. Furthermore absorption bands in the region of perturbed OH stretching vibrations (3400-3000 cm^{-1}) are formed only at 400°C.

Finally, **??** shows the IR absorption spectra collected after exposure to the same total amount of SO_2 but different concentrations, *i.e.*, 10 ppm for 15 min, 30 ppm for 5 min and 50 ppm for 3 min in the presence of O_2, are directly compared. The SO_2 exposure corresponds to a total amount of 0.67 μmol SO_2. Interestingly, the spectra collected during experiments performed at the same temperature with different SO_2 concentrations do not overlap, indicating that the effects of SO_2 exposure depend on the SO_2 concentration in the feed gas mixture. In particular, the highest intensity for the absorption bands related to sulfates on silica (around 1430 cm^{-1}) is observed for the lowest (10 ppm) and the highest (50 ppm) SO_2 concentrations at 200-300°C and 400°C, respectively.

SO_x adsorption on silica, platinum and diamond

The difference absorption spectra collected at the end of each experiment performed on the SiO_2 diluted in diamond are reported in Figure S3a. The absence of absorption bands at all temperatures suggests that the species adsorbed on the silica surface prior to the experiments are not modified upon the SO_2 exposure. The spectra collected at the end of each experiment for Pt black diluted with diamond (after 15 min of exposure to 50 ppm SO_2, and further 15 min in the presence of 50 ppm SO_2 and 10% O_2) are reported in Figure S3b. In all experiments with Pt black the most significant changes are observed in the wavenumber region 1350-1200 cm^{-1}. Two overlapping absorption bands appear at 1336-1328 and 1237 cm^{-1} upon SO_2 exposure at 200 and 300°C. We assign the first band to SO_2 adsorbed on the surface of either diamond or the reaction cell[28] and the second to *trans*-HSCS species.[32] An absorption band at 1287 cm^{-1} accompanies that at 1232 cm^{-1} upon SO_2 exposure at 400°C, which might be related to the HCS deformation of *trans*-

dithioformic acid (HCSSH)[32,38] or to SO_2 adsorbed on Pt.[34] We mention that no sulfur containing species on platinum could be detected under oxygen-free conditions (not shown). The absorption bands at 3261 and 2990 cm^{-1} are not straightforward to assign but might be related to some form of C-H stretching.[37] However, even if unlikely (see discussion), a contribution of the KBr windows and/or impurities present in the DRIFTS reaction cell cannot be excluded.

Computed energetic and structural data

The optimized structure of gaseous sulfur oxides (SO_2, SO_3) or sulfate (SO_4^{2-}) on the Pt surface presents an oxygen atom of the adsorbate bonded to the Pt surface with a Pt-O distance around 2.12-2.46 Å, in agreement with previous studies of SO_2 adsorption on a Pt surface.[39] As the number of oxygen atoms bonded to the sulfur atom increases, the interaction becomes stronger, as shown in **??**. The interaction energies of sulfur oxides with the Pt_4 cluster and the Pt surface are significantly different due to the under-coordinated state of platinum in the Pt cluster.[22]

In the case of SO_2 adsorption on SiO_2, two different scenarios are considered: SO_2 interacts with a hydroxyl group by forming either an intermolecular or an intramolecular bond. In the first case, a hydrogen bond is formed between the hydrogen in the hydroxyl group and the oxygen in SO_2. The interaction is relatively weak, 0.17 eV for the $Si(OH)_4$ cluster and 0.24 eV for the β-Cristobalite cluster. In this case, the difference in adsorption energy between the two clusters is not significant due to the absence of chemical reactions. In the second scenario, SO_2 reacts with a hydroxyl group to form two additional covalent O-S bonds. The result is the formation of a sulfate-like species on the surface of SiO_2, more strongly bonded, 1.56 eV for the $Si(OH)_4$ cluster and 2.48 eV for the β-Cristobalite cluster. The same is the case for SO_2 interaction with Pt, the difference in adsorption energy becomes more pronounced when intramolecular bonds are formed between sulfur oxides and SiO_2.

Computed IR vibrational spectra

The results of the calculations of the vibrational spectra of gaseous sulfur oxides (SO_2, SO_3) and sulfate (SO_4^{2-}) on Pt clusters are shown in **??** and **??**. More details on the computed spectra are given in the supporting information. Although most of the vibrational frequencies appear at wavenumbers lower than 1200 cm^{-1}, some features can be found between 1200 and 1300 cm^{-1}, corresponding to Pt-O vibrational modes as shown in **??**a. This is the case of the larger Pt cluster, where oxygen adsorb on the top of Pt atoms, whereas the smaller Pt cluster cannot provide enough Pt sites for the O from SO_2 or SO_3 to be adsorbed on top.

More phenomena can be observed for the SO_2 adsorption on SiO_2 in **??**. Selected figures illustrating SO_2-SO_3 interactions are displayed in **??**a and b. In agreement with the DRIFTS experiments, a peak around 1310-1440 cm^{-1} is obtained for the sulfate-like compounds on the surface of SiO_2. Most of the less pronounced peaks in the calculations (around 1300 cm^{-1}) are related to the presence of physisorbed SO_2 on the SiO_2 surface. Peaks around 1420 and 1440 cm^{-1} are obtained for chemisorption and sulfate formation as shown in **??**b. Vibrations related to silanol groups can also be observed around 3700-3900 cm^{-1} with lower intensity. The O-H vibrational modes of the hydrogen bond can also be observed above 3000 cm^{-1} as illustrated in **??**c. In addition, some peaks are also obtained between 3000 and 3200 cm^{-1} in the presence of hydrogen bonds. Strong hydrogen bonds, such as those in the interacting $Si(OH)_4$-SO_4^{2-} (where three of such bonds are formed), result in increased intensity of the peak at 3000 cm^{-1}. Hydrogen bond interactions are also obtained in the presence of H_2SO_4 on the surface of SiO_2, which is characterized by peaks between 3400 and 3600 cm^{-1}.

Additional calculations were performed for the Pt-H and the SO_2-diamond systems to investigate whether spillover of hydrogen atoms from the oxide to the metal is possible and the SO_2 interaction with carbon, respectively. The results are shown in Figure S7. A Pt-H bond should generate a peak at 2295 cm^{-1}, which is not observed experimentally. Thus the computations do not support the possibility of hydrogen spillover to the Pt surface. A C-S bond should result in an absorption band around 1300 cm^{-1}, which might explain the peak observed in the experiment

with Pt black diluted with diamond. However, the intensity for these peaks is very low. Indeed, these peaks might also originate from Pt-sulfur interactions (1200-1300 cm^{-1}). In the case of diamond less intense peaks can also be observed at 1100 cm^{-1} for C-C bonds, at 1300-1400 cm^{-1} and around 3000 cm^{-1} for C-H bonds.

Discussion

In order to allow for a fair comparison of the results, all DRIFTS experiments have been performed using one single sample of 4% Pt/SiO_2. Although the development of a sample regeneration procedure is beyond the present scope, it is worth to spend a few words on this before discussing the results. Different strategies for cleaning of the surface after each SO_2 adsorption experiment have been tested. Purging the sample with Ar or 10% O_2 in Ar at 200°C showed to be insufficient as well as heating the sample to 400°C in an Ar flow. On the contrary, feeding 4% H_2 in Ar made most of the IR absorption bands detected in presence of SO_2 to disappear, which means that the species adsorbed on the surface of the sample are removed. This is also in-line with previous studies where treatments under various reducing atmospheres were reported to efficiently remove sulfur species from sulfur-poisoned catalysts.[40,41] The efficiency of the regeneration procedure used in the present study is further proved by the overlap of the reference spectra collected prior to each experiment (*cf.* **??**). Therefore concerns about the comparability of the results of different experiments can be ruled out, as a common starting point was found for the Pt/SiO_2 surface.

A second issue that might influence the results is the fact that the Pt/SiO_2 sample has been diluted with diamond powder. The need of a transparent diluent is unquestionable as silica absorbs strongly in the infrared region between 1600 and 1000 cm^{-1}, which coincides with the fingerprint region for sulfur containing species.[37] The most common diluents used in IR spectroscopic studies are alkali halides such as potassium bromide (KBr). However, these alkali salts might react with SO_2 in the gas phase and form potassium sulfate (K_2SO_4), giving rise to undesired IR absorption bands.[38,42] An absorption band at 1140 cm^{-1}, accompanied by a less intense band at 1265 cm^{-1},

has been observed in our lab when exposing a KBr powder sample mixed with 1 wt.% platinum black to several SO_2/O_2 gas mixtures. When only SO_2 was present in the feed, a double band at 1378 and 1353 cm^{-1} was observed, which is typical of gaseous SO_2. In the light of these results, we might consider a contribution of the KBr windows unlikely in our experiments, since they are exposed only to SO_2 in the gas phase, whereas gaseous SO_3 can be formed only by oxidation of SO_2 on active platinum sites in the catalytic bed. However the use of KBr as diluent for the Pt/SiO_2 sample would likely give rise to undesired IR absorption bands. To our purpose, it was therefore preferable to use a transparent non-reactive material, such as diamond,[43,44] as diluent. Blank experiments have been performed using diamond powder, which was mixed with platinum black in order to allow the occurrence of the catalytic oxidation of SO_2 to SO_3. The results (*cf.* Figure S3) clearly show that the contribution of the diluent and of the reaction cell is negligible for wavenumbers above 1350 cm^{-1}, exception made by the absorption bands at 3261 and 2990 cm^{-1}, which can be assigned to some form of C-H stretching, as suggested by calculations (*cf.* Figure S7). On the contrary, all the absorption bands detected in the IR region 1350-1200 cm^{-1} for the Pt/SiO_2 sample also appear in the corresponding blank experiment, with comparable intensities. Thus we might confidently suggest that sulfur-platinum and/or sulfur-carbon (either from the diamond diluent or the interior of the stainless steel reaction cell) interactions are established during the experiments. This is also in agreement with calculations (*cf.* Figure S4). In the light of these results, only absorption bands above 1350 cm^{-1} will be considered in the following discussion of the experiments for the Pt/SiO_2 sample, together with the peak at 1286 cm^{-1} that we assign to the Pt-O vibration frequency for sulfate on platinum.

It is generally recognized that silica surfaces are terminated with either oxygen from siloxane groups or OH from one of several forms of silanol groups (**??**). The latter could be i) *geminal*; two silanol groups attached to the same silicon atom, ii) *isolated*; free silanol groups not interacting with each other or iii) *vicinal*; two silanol groups attached to two different silicon atoms bridged by an H-bond.[45] In principle, when performing a DRIFTS study, one should be able to distinguish between these species since they present different vibrational frequencies. A broad absorption

band between 3600 and 3450 cm^{-1} is characteristic for *vicinal* silanols,[13] whereas when *isolated* or *geminal* silanols are present on the surface sharp absorption bands appear at 3720[26] and 3742 cm^{-1},[31] respectively. However, OH stretching vibrations of *vicinal* silanols overlap with those of adsorbed water.[13,22,29,35] Furthermore, upon exposure of the surface to different species in the gas phase, interactions between silanols and adsorbates can be established, which might give rise to shifts in the positions of the absorption bands. In the following we will refer to these species as perturbed silanol groups.

The DRIFTS experiments clearly show that the formation of sulfates on the silica surface (1430 cm^{-1}) is accompanied by removal of both *isolated* (3730 cm^{-1}) and *vicinal* silanols (3530 cm^{-1}) for all temperatures investigated. Simultaneously, a rearrangement of the remaining silanols, promoted by the steric hindrance of the newly formed sulfates might occur, as suggested by the appearance of a positive absorption band at 3745 cm^{-1} (*geminal* silanols). Furthermore, the formation of H-bonds between silanols and sulfates adsorbed in their vicinities (perturbed silanols in **??**) is possible, which might contribute to the appearance of broad bands between 3200 and 3000 cm^{-1}. However, since these bands are observed also on the blank experiments performed on diamond powder, the major contribution in this wavenumber region is likely to come from stretching vibration mode of C-H bonds. This possibility is also supported by the computational results, where peaks around 3082 cm^{-1} were calculated for C-H vibration (*cf.* Figure S7). Experimental results clearly show that platinum plays a major role in the storage mechanism. It has been shown that the presence of platinum can enhance the performance of ceria-based SO_x traps, which is explained by the formation of SO_3 over noble metal sites and the subsequent spillover to the support.[46,47] In the present study, both the IR spectra (**??**) and the integrated peak areas for sulfates on silica and terminal silanols (**??**) indicate that the SO_x storage process occurs only in the presence of oxygen in the feed gas. Moreover, no surface species are formed/removed during blank experiments performed on bare SiO_2, neither in absence nor in presence of O_2 (Figure S4a). These findings are also supported by quantum chemical calculations, which indicate that SO_2 only interacts weakly with SiO_2 (0.17-0.28 eV in **??**), while SO_3 and SO_4 can be chemically absorbed (1.48-2.48 eV

in **??**). This suggests that catalytic oxidation of SO_2 to SO_3 on platinum sites is a first necessary step in the formation of sulfates. Moreover, platinum might also play a second indirect role in the SO_x storage mechanism on silica, by providing dissociated hydrogen species for the formation of terminal silanols during the reducing pre-treatment.[13]

Another important information that we can obtain from the IR spectra is that the nature of the surface sulfates formed on silica neither is dependent on the temperature at which the experiment has been performed nor on the SO_2 concentration used, since the same absorption band at 1430 cm^{-1} is observed for all experiments. However, the amount of sulfates that form on silica depends on the SO_2 concentration in the gas phase. This is especially clear from the IR spectra displayed in **??**, showing a direct comparison between spectra collected after exposure of the sample to different concentrations but the same total amount of SO_2. Furthermore, the amount of sulfates formed depends also on the temperature, with the higher intensity for the IR band related to sulfates on silica (1430 cm^{-1}) always obtained at the end of the experiments performed at 300°C, which is in agreement with the sensing measurement on Pt-gate sensors performed previously.[6] This might be explained considering that the adsorption process is a compromise between kinetics and thermodynamics, with higher temperatures enhancing the rate of SO_x adsorption but limiting the amount of SO_x that can be stored. This is also consistent with the asymptotic trends observed for the integrated area of sulfates on silica at 300 and 400°C, indicating that saturation was approached during the corresponding experiments.

Conclusions

In the present study the interaction between SO_2 and Pt/SiO_2 and subsequent formation of ad-SO_x species has been studied using *in situ* DRIFT spectroscopy. Additionally, first principle calculations have been performed to support the assignment of the absorption bands observed experimentally. The results show that oxygen is required in order to form sulfate species (both on the metal and on the support material) and that the formation of sulfates on the silica surface always

is associated with removal/rearrangement of silanol groups. Furthermore, no surface species are formed/removed during blank experiments performed on the bare SiO_2 (neither in absence nor in presence of O_2). The calculation results also indicate that intramolecular bonds are less likely to be formed between SO_2 and bare SiO_2. These findings support the idea of SO_2 oxidation to SO_3 over the noble metal as a necessary first step in the process of sulfate formation, likely followed by spillover of SO_3 to the support and formation of ${SO_4}^{2-}$ species in hydroxyl positions. For the understanding of the sensing mechanism this suggests that a polarized layer of SO_4^{2-} species can be formed on the silica surface, which can modify the electrical behavior of the device. The results also indicate that the sulfate formation on silica is temperature dependent and peaks at 300°C, while perturbed silanol groups only seem to be formed at 400°C. Interestingly, the effect of SO_2 exposure in the DRIFT experiments depends on the SO_2 concentration in the feed gas mixture. The highest intensity for the absorption bands related to sulfates on silica was observed for the lowest (10 ppm) and the highest (50 ppm) SO_2 concentrations at all investigated temperatures.

Acknowledgements

This study has been performed at the Competence Centre for Catalysis, which is financially supported by Chalmers University of Technology, the Swedish Energy Agency and the member companies: AB Volvo, ECAPS AB, Haldor Topsøe A/S, Scania CV AB, Volvo Car Corporation AB and Wärtsilä Finland Oy. The quantum-chemical calculation part of this work was supported by National Supercomputer Center (NSC), as part of Swedish National Infrastructure for Computing (SNIC), and funded by Swedish Research Council (VR).

Supporting Information Available

The experimental results (Figures S1-S2), computed spectra (Figures S3-S6) and convergence test (Tables S1-S3) are included in Supporting Information. This information is available free of charge via the Internet at http://pubs.acs.org.

References

(1) Andersson, M.; Pearce, R.; Spetz, A. L. New Generation SiC Based Field Effect Transistor Gas Sensors. *Sens. Actuators B: Chem.* **2013**, *179*, 95–106.

(2) Lundström, I.; Sundgren, H.; Winquist, F.; Eriksson, M.; Krantz-Rücker, C.; Spetz, A. L. Twenty-Five Years of Field Effect Gas Sensor Research in Linköping. *Sens. Actuators B: Chem.* **2007**, *121*, 247–262.

(3) Wingbrant, H.; Svenningstorp, H.; Salomonsson, P.; Kubinski, D.; Visser, J. H.; Löfdahl, M.; Spetz, A. L. Using a MISiC-FET Sensor for Detecting NH_3 in SCR Systems. *IEEE Sensors J.* **2005**, *5*, 1099–1105.

(4) Andersson, M.; Ljung, P.; Mattsson, M.; Löfdahl, M.; Spetz, A. L. Investigations on the Possibilities of a MISiCFET Sensor System for OBD and Combustion Control Utilizing Different Catalytic Gate Materials. *Top. Catal.* **2004**, *30/31*, 365–368.

(5) Andersson, M.; Everbrand, L.; Spetz, A. L.; Nyström, T.; Nilsson, M.; Gauffin, C.; Svensson, H. A MISiCFET Based Gas Sensor System for Combustion Control in Small-Scale Wood Fired Boilers. *IEEE Sensors* **2007**, 962–965.

(6) Darmastuti, Z.; Bur, C.; Möller, P.; Rahlin, R.; Lindqvist, N.; Andersson, M.; Schütze, A.; Spetz, A. L. SiC-FET based SO_2 Sensor for Power Plant Emission Applications. *Sens. Actuators B: Chem.* **2014**, *194*, 511–520.

(7) Dobos, K.; Armgarth, M.; Zimmer, G.; Lundström, I. The Influence of Different Insulators on Palladium-Gate Metal-Insulator-Semiconductor Hydrogen Sensors. *IEEE Trans. Electron Devices* **1984**, *31*, 508–510.

(8) Darmastuti, Z.; Pearce, R.; Spetz, A. L.; Andersson, M. The Influence of Gate Bias and Structure on the CO Sensing Performance of SiC Based Field Effect Sensors. *Sensors IEEE* **2011**, 133–136.

(9) Löfdahl, M.; Utaiwasin, C.; Carlsson, A.; Lundström, I.; Eriksson, M. Gas Response Dependence on Gate Metal Morphology of Field-Effect Devices. *Sens. Actuators B: Chem.* **2001**, *80*, 183–192.

(10) Nakagomi, S.; Takahashi, M.; Unéus, L.; Savage, S.; Wingbrandt, H.; Andersson, M.; Lundström, I.; Löfdahl, M.; Spetz, A. L. Substrate Bias Amplification of a SiC Junction Field Effect Transistor With a Catalytic Gate Electrode. *Materials Science Forum* **2004**, 1507–1510.

(11) Nakagomi, S.; Fukumura, A.; Kokubun, Y.; Savage, S.; Wingbrant, H.; Andersson, M.; Lundström, I.; Löfdahl, M.; Spetz, A. L. Influence of Gate Bias of MISiC-FET Gas Sensor Device on the Sensing Properties. *Sens. Actuators B: Chem.* **2005**, *108*, 501–507.

(12) Lundström, I.; DiStefano, T. Hydrogen Induced Interfacial Polarization at PdSiO_2 Interfaces. *Surf. Sci.* **1976**, *59*, 23–32.

(13) Wallin, M.; Grönbeck, H.; Spetz, A. L.; Eriksson, M.; Skoglundh, M. Vibrational Analysis of H_2 and D_2 Adsorption on Pt/SiO_2. *J. Phys. Chem. B* **2005**, *109*, 9581–9588.

(14) Wallin, M.; Byberg, M.; Grönbeck, H.; Skoglundh, M.; Eriksson, M.; Spetz, A. L. Vibrational Analysis of H_2 and NH_3 Adsorption on Pt/SiO_2 and Ir/SiO_2 Model Sensors. *IEEE Sensors* **2007**, *1-3*, 1315–1317.

(15) Becker, E.; Andersson, M.; Eriksson, M.; Spetz, A. L.; Skoglundh, M. Study of the Sensing Mechanism Towards Carbon Monoxide of Platinum-Based Field Effect Sensors. *IEEE Sensors J.* **2011**, *11*, 1527–1534.

(16) Bounechada, D.; Fouladvand, S.; Kylhammar, L.; Pingel, T.; Olsson, E.; Skoglundh, M.; Gustafson, J.; Michiel, M. D.; Newton, M. A.; Carlsson, P.-A. Mechanisms Behind Sulfur Promoted Oxidation of Methane. *Phys. Chem. Chem. Phys.* **2013**, *15*, 8648–8661.

(17) Brunelle, J. P. Preparation of Catalysts by Metallic Complex Adsorption on Mineral Oxides. *Pure Appl. Chem.* **1978**, *50*, 1211–1229.

(18) Frisch, M. J.; Trucks, G. W.; Schlegel, H. B.; Scuseria, G. E.; Robb, M. A.; Cheeseman, J. R.; Montgomery, J. A., Jr.; Vreven, T.; Kudin, K. N.; Burant, J. C.; et al., Gaussian 03, Revision C.02. Gaussian, Inc., Wallingford, CT, 2004.

(19) Parr, R. G.; Yang, W. Density-Functional Theory of the Electronic Structure of Molecules. *Ann. Rev. Phys. Chem.* **1995**, *46*, 701–28.

(20) Hehre, W. J.; Ditchfield, K.; Pople, J. A. Self-Consistent Molecular Orbital Methods. XII. Further Extensions of Gaussian-Type Basis Sets for Use in Molecular Orbital Studies of Organic Molecules. *J. Chem. Phys.* **1972**, *56*, 2257–2261.

(21) Hay, P. J.; Wadt, W. Ab Initio Effective Core Potentials for Molecular Calculations. Potentials for the Transition Metal Atoms Sc to Hg. *J. Chem. Phys.* **1985**, *82*, 270–283.

(22) Wallin, M.; Grönbeck, H.; Spetz, A. L.; Skoglundh, M. Vibrational Study of Ammonia Adsorption on Pt/SiO_2. *Appl. Surf. Sci.* **2004**, *235*, 487–500.

(23) Flikkema, E.; Jelfs, K. E.; Bromley, S. T. Structure and Energetics of Hydroxylated Silica Clusters, (SiO_2) M(H_2O) N, M = 8, 16 and N = 1 - 4: A Global Optimization Study. *Chem. Phys. Lett.* **2012**, *554*, 117–122.

(24) Konicek, A. R.; Grierson, D. S.; Sumant, A. V.; Friedmann, T. A.; Sullivan, J. P.; Gilbert, P. U. P. A.; Sawyer, W. G.; Carpick, R. W. Influence of Surface Passivation on the Friction and Wear Behavior of Ultrananocrystalline Diamond and Tetrahedral Amorphous Carbon Thin Films. *Phys. Rev. B* **2012**, *85*.

(25) Anderson, B. G.; Dang, Z.; Morrow, B. Silica-Supported Zirconia. 2. Effect of Sulfation on the Surface Acidity and Its Potential as a Catalyst for Methane-Olefin Coupling. *J. Phys. Chem.* **1995**, *99*, 14444–14449.

(26) Morrow, B. A.; McFarlan, A. J. Infrared and Gravimetric Study of an Aerosil and a Precipitated Silica Using Chemical and H/D Exchange Probes. *Langmuir* **1991**, *7*, 1695–1701.

(27) Bailie, J. E.; Rochester, C.; Hutchings, G. Effects of Thiophene and Sulfur Dioxide on CO Adsorption on Cobalt/Silica Catalysts. *J. Chem. Soc. Farad. Trans.* **1997**, *93*, 2331–2336.

(28) Zawadzki, J. Infrared Studies of SO_2 on Carbons - I. Interaction of SO_2 With Carbon Films. *Carbon* **1987**, *25*, 431–436.

(29) Verwilghen, C.; Guilet, R.; Deydier, E.; Menu, M. J.; Dartiguenave, Y. Lead and Cadmium Uptake by Sulfur-Containing Modified Silica Gels. *Environ. Chem. Lett.* **2004**, *2*, 15–19.

(30) Busca, G. The Surface Acidity of Solid Oxides and Its Characterization by IR Spectroscopic Methods. An Attempt at Systematization. *Phys. Chem. Chem. Phys.* **1999**, *1*, 723–736.

(31) Iwasawa, Y. In *Tailored Metal Catalysts*; Iwasawa, Y., Ed.; D. Riedel, Dordrecht, Holland, 1986.

(32) Bohn, R. B.; Brabson, G.; Andrews, L. Reaction of Atomic Hydrogen and Carbon Disulfide: Infrared Spectra of HSCS and HSHCS in Solid Argon. *J. Phys. Chem.* **1992**, *96*, 1582–1589.

(33) Schnöckel, H. Matrixisolation von OSiS: IR-Spektroskopischer Nachweis Einer Si-S-Doppelbindung. *Angew. Chem.* **1980**, *92*, 310–313.

(34) Moraes, I. R.; Weber, M.; Nart, F. On the Structure of Adsorbed Sulfur Dioxide at the Platinum Electrode. *Electrochim. Acta* **1997**, *42*, 617–625.

(35) Zholobenko, V. L.; Kustov, L. M.; Borovkov, V. Y.; Kazansky, V. B. A New Type of Acidic Hydroxyl Groups in ZSM-5 Zeolite and in Mordenite According to Diffuse Reflectance IR Spectroscopy. *Zeolites* **1988**, *8*, 175–178.

(36) Karyakin, A. V.; Muradova, G.; Maisuradze, G. IR Spectroscopic Study of the Interaction of Water With Silanol Groups. *J. Appl. Spetrosc.* **1970**, *12*, 675–677.

(37) Silverstein, R. M.; Bassler, G. C.; Morrill, T. *Spectrometric Identification of Organic Compounds*, 4th ed.; Wiley, Singapore, 1981.

(38) Ioannoni, F.; Moule, D. C.; Goddard, J. D.; Clouthier, D. J. Thiocarbonyl Spectroscopy: The Infrared Spectrum and Ab Initio Vibrational Frequencies of Cis- and Trans-Dithioformic Acid in the $X^1$1A' Ground State. *J. Mol. Struc.* **1989**, *197*, 159–170.

(39) Lin, X.; Schneider, W. F.; Trout, B. L. Chemistry of Sulfur Oxides on Transition Metals III. Oxidation of $SO_2$2 and Self-Diffusion of O, SO_2, and SO_3 on Pt(111). *J. Phys. Chem. B* **2004**, *108*, 13329–13340.

(40) Hoyos, L. J.; Praliaud, H.; Primet, M. Catalytic Combustion of Methane Over Palladium Supported on Alumina and Silica in Presence of Hydrogen Sulfide. *Appl. Catal. A Gen.* **1993**, *98*, 125–138.

(41) Mathieu, M. V.; Primet, M. Sulfurization and Regeneration of Platinum. *Appl. Catal.* **1984**, *9*, 361–370.

(42) Peralta, M. A.; Milt, V. G.; Cornaglia, L. M.; Querini, C. A. Stability of Ba,K/CeO_2 Catalyst During Diesel Soot Combustion: Effect of Temperature, Water, and Sulfur Dioxide. *J. Catal.* **2006**, *242*, 118–130.

(43) TeVrucht, M. L. E.; Griffiths, P. Quantitative Investigation of Matrices for Diffuse Reflectance Infrared Fourier Transform Spectrometry. *Talanta* **1991**, *38*, 839–849.

(44) Brackett, J. M.; Azarraga, L. V.; Castles, M. A. Matrix Materials for Diffuse Reflectance Fourier Transform Infrared Spectrometry of Substances in Polar Solvents. *Anal. Chem.* **1984**, *56*, 2007–2010.

(45) Kiselev, A. V.; Lygin, V. I. *Infrared Spectra of Surface Compounds*; Wiley, New York, 1975.

(46) Kylhammar, L.; Carlsson, P.-A.; Ingelsten, H. H.; grönbeck, H.; Skoglundh, M. Regenerable

Ceria-Based SO_x Traps for Sulfur Removal in Lean Exhausts. *Appl. Catal. B Environ.* **2008**, *84*, 268–276.

(47) Happel, M.; Kylhammar, L.; Carlsson, P.-A.; Libuda, J.; Grönbeck, H.; Skoglundh, M. SO_x Storage and Release Kinetics for Ceria-Supported Platinum. *Appl. Catal. B Environ.* **2009**, *91*, 679–682.

() Meriaudeau, P.; Thangaraj, A.; Naccache, C.; Narayanan, S. Interaction of Hydrogen With Pt-Silicalite. *J. Catal.* **1994**, *148*, 617–624.

() Gallas, J. P.; Goupil, J. M.; Vimont, A.; Lavalley, J. C.; Gil, B.; Gilson, J. P.; Miserque, O. Quantification of Water and Silanol Species on Various Silicas by Coupling IR Spectroscopy and in-Situ Thermogravimetry. *Langmuir* **2009**, *25*, 5825–5834.

Figures and Tables

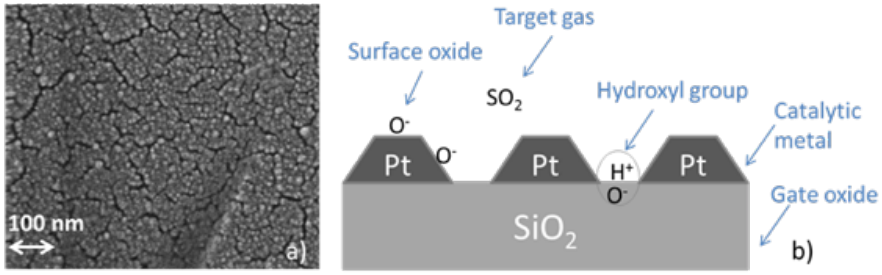

Figure 1: SiC-FET surface: a) SEM micrograph of the Pt porous surface, b) schematic cross-section view of the sensor surface.

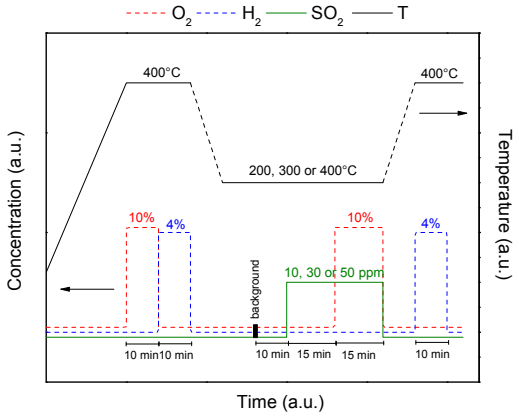

Figure 2: Schematic description of the isothermal SO_2 exposure DRIFTS experiment with the collection point of the background spectra.

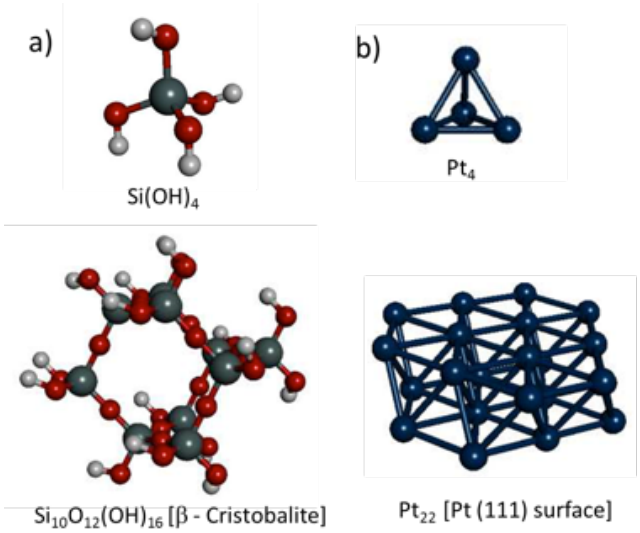

Figure 3: Optimized geometry of the a) SiO_2 and b) Pt clusters employed for the quantum chemical calculations for energies and vibrational spectra. Color code: blue for Pt, grey for Si, red for O, and white for H.

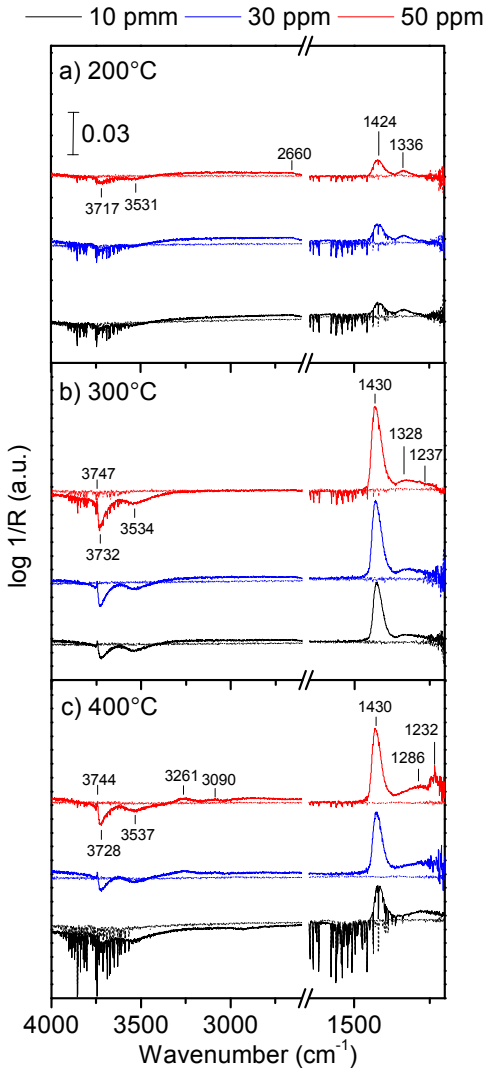

Figure 4: Difference IR absorption spectra for the Pt/SiO_2 sample collected at a) 200, b) 300 and c) 400°C after 15 min of exposure to SO_2 (dotted lines) and after further 15 min of exposure to SO_2 in the presence of 10% O_2 (solid lines) (100 ml/min of total flow).

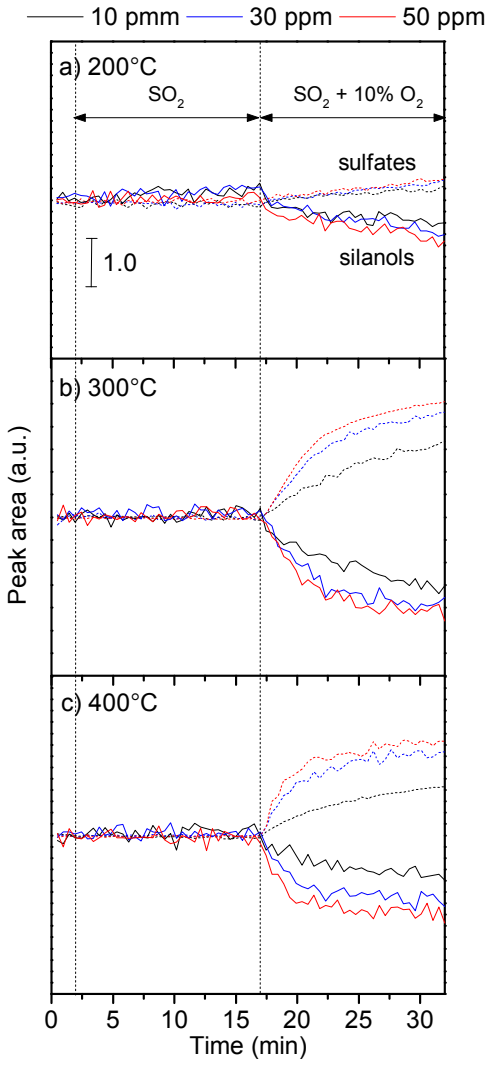

Figure 5: Integrated peak areas between 1480 and 1350 cm^{-1} representing sulfates on silica (dashed lines) and between 3900 and 3400 cm^{-1} representing silanols (solid lines) for the experiments at a) 200, b) 300 and c) 400°C.

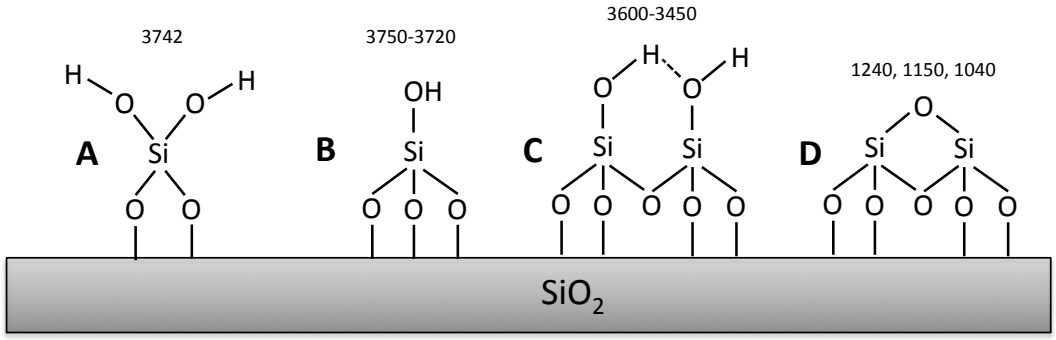

Figure 6: Schematic representation of terminal silanol and siloxane groups on silica surfaces: A) *geminal*, B) *isolated* and C) *vicinal* (H-bonded) silanols, and D) siloxane. Characteristic wavenumbers are also shown for these species.

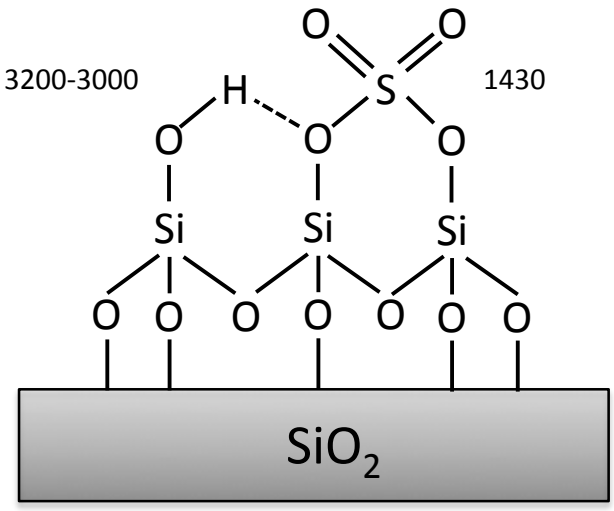

Figure 7: Tentative representation of a surface sulfate on silica and of its interaction with a *vicinal* OH group (perturbed silanol). Characteristic wavenumbers are also shown for these species.

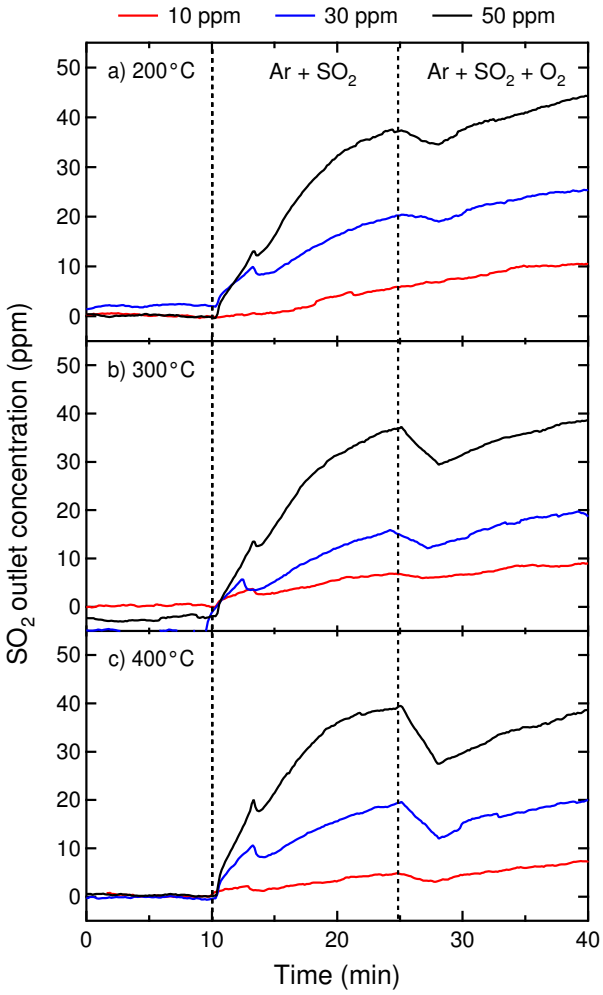

Figure 8: Outlet SO_2 concentration profiles (m/z 64) detected during the SO_2 exposure experiments performed at a) 200, b) 300 and c) 400°C on 4% Pt/SiO_2.

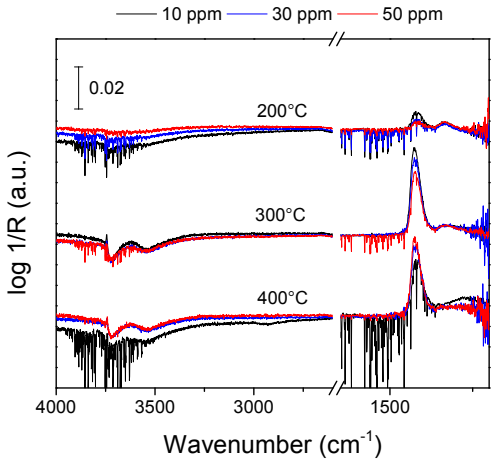

Figure 9: Difference IR absorption spectra for the Pt/SiO_2 sample collected at 200, 300 and 400°C after exposure to the same amount of SO_2 (6.69e-7 mol) in the presence of O_2.

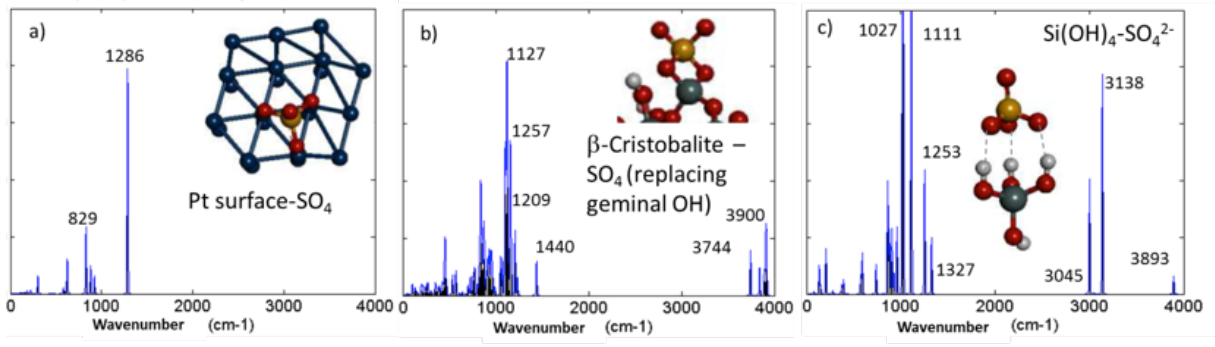

Figure 10: Selected pictures of the computed spectra for a) SO_4^{2-} on top of Pt(111) surface, b) SO_4-like species on the geminal termination on β-Cristobalite cluster and c) SO_4^{2-} interaction with $Si(OH)_4$ cluster. More information can be found in the supporting information (Figure S3-S6).

Table 1: Summary of infrared band positions for sulfur-containing species, water and silanol groups assigned in the open literature.

Assignment	Absorption band (cm^{-1})	Reference
S-containing species		
Gaseous SO	1149	[38]
Gaseous SO_2	1362, 1151, 518	[38]
Gaseous SO_3	1391, 1065, 530, 498	[38]
Silicon oxysulfide (OSiS)	1290, 1265, 643	[33]
Surface sulfate on SiO_2	1343, 1440, 1425	[25,27]
Thiol (SiSH)	2580	[34]
SO_2 adsorbed on Pt (ponte)	1160-1100, 950-850	[34]
SO_2 adsorbed on Pt (pyramidal)	1225-1150, 1065-990	[34]
SO_2 adsorbed on Pt (bridging)	1240-1135, 1085-975	[34]
SO_2 adsorbed on Pt (planar)	1300-1125, 1140-1045	[34]
Water species		
Condensed	1620	[25]
	1630	[13]**?**
Adsorbed	3441	[29]
	3500, 3450	[22]
	3600	**?**
	3665, 3450, 3100-3000	[36]
Gaseous	3950-3550, 1900-1350	[13]
Silanol species		
Si-OH	3800-3200	[26]
Internal Si-OH (H-bonded)	3250	[35]
vicinal Si-OH (H-bonded)	3520	[26]**?**
	3610	[35]
isolated Si-OH	3739	[29]
	3740	[13,22,35]
	3747	[25]
	3747-3737, 3720	[26]
	3750-3730	[30]
geminal Si-OH	3742	[31]

Table 2: Energetic and structural data obtained from quantum chemical calculations for SO_2 and oxidized SO_2 on the surface of Pt_4, Pt_{22} (Pt 1 1 1), $Si(OH)_4$, and $Si_{10}O_{12}(OH)_{16}$ (β-Cristobalite) with different terminations. E_{ads} was calculated as the difference between the energy of the product and the sum of the energy of the reactants.

Species	E_{ads} (eV)	d (Å)
Pt_4-SO_2	0.91	2.21
Pt_4-SO_3	1.38	2.18
Pt_4-SO_4	6.48	2.12
Pt_{22}-SO_2	0.44	2.46
Pt_{22}-SO_3	2.18	2.19
Pt_{22}-SO_4	2.85	2.14
$Si(OH)_4$-SO_2	0.17	2.87
$Si(OH)_4$-SO_3	0.38	2.37
$Si(OH)_4$-SO_4	1.40	2.79
$Si(OH)_2$-SO_4	1.56	1.69
SiO_2 (*geminal*)-SO_4	2.48	1.64
SiO_2 (*geminal*)-H-SO_4	0.24	2.84
SiO_2 (*isolated*)-SO_3	1.48	2.11
SiO_2 (*isolated*)-H-SO_3	0.28	3.56
SiO_2 (siloxane)-SO_4	0.17	2.30

Table 3: Summary of infrared band positions for sulfur-containing species, water and silanol groups assigned in the open literature.

System	Vibration	Calculated wavenumber (cm^{-1})
Pt_4-SO_2	S-O-Pt stretch	901, 1007
Pt_4-SO_3	S-O-Pt vibration	642, 885
Pt_4-SO_4	S-O-Pt stretch	986, 1193, 1297
Pt_{22}-SO_2	S-O-Pt stretch	1164, 1299
Pt_{22}-SO_3	S-O-Pt stretch	784-859
Pt_{22}-SO_4	S-O-Pt stretch	829, 1286
$Si(OH)_4$-SO_2	O-H vibration	1008
	S-O-Si-O vibration	1321
	isolated O-H stretch	3800-3900
$Si(OH)_4$-SO_3	O-H vibration	1002, 1037, 1049
	S-O-Si-O vibration	1337, 1366
	O-H (isolated) stretch	3800-3900
$Si(OH)_4$-$SO_4{}^{2-}$	O-H vibration	999, 1027
	S-O stretch	1111
	S-O-Si-O vibration	1327
	O-H stretch	3045, 3138
	O-H (isolated) stretch	3800-3900
$Si(OH)_4$-H_2SO_4	O-H vibration in $Si(OH)_4$ and H_2SO_4	1018, 1045, 1181, 1339
	S-O stretch	1157
	S-O vibration in sulfate	1443
	O-H stretch	3410, 3592
	O-H (isolated) stretch	3800-3900
$Si(OH)_2(O)_2$-SO_2	O-H vibration	1003, 1041
($SO_4{}^{2-}$ like)	S-O stretch	1205
	S-O asymmetric stretch and S-Si twist	1368
	O-H (geminal) stretch	3735
	O-H (isolated) stretch	3700-3900
β-Cristobalite cluster-SO_2	O-H vibration	1000-1127
(geminal site)	S-O stretch	1209-1257
	S-O asymmetric stretch and S-Si twist	1440
	O-H (geminal) stretch	3744
	O-H (isolated) stretch	3700-3900
β-Cristobalite cluster-SO_2	O-H vibration	1170
(isolated site)	S-O stretch	1216-1310
	O-H (geminal) stretch	3750
	O-H (isolated) stretch	3700-3900